


Increased biomass and carbon burial 2 billion years ago triggered mountain building

John Parnell ¹✉ & Connor Brolly¹

The geological record following the c. 2.3 billion years old Great Oxidation Event includes evidence for anomalously high burial of organic carbon and the emergence of widespread mountain building. Both carbon burial and orogeny occurred globally over the period 2.1 to 1.8 billion years ago. Prolific cyanobacteria were preserved as peak black shale sedimentation and abundant graphite. In numerous orogens, the exceptionally carbonaceous sediments were strongly deformed by thrusting, folding, and shearing. Here an assessment of the timing of Palaeoproterozoic carbon burial and peak deformation/metamorphism in 20 orogens shows that orogeny consistently occurred less than 200 million years after sedimentation, in a time frame comparable to that of orogens through the Phanerozoic. This implies that the high carbon burial played a critical role in reducing frictional strength and lubricating compressive deformation, which allowed crustal thickening to build Palaeoproterozoic mountain belts. Further, this episode left a legacy of weakening and deformation in 2 billion year-old crust which has supported subsequent orogenies up to the building of the Himalayas today. The link between Palaeoproterozoic biomass and long-term deformation of the Earth's crust demonstrates the integral relationship between biosphere and lithosphere.

¹School of Geosciences, University of Aberdeen, Aberdeen AB24 3UE, United Kingdom. ✉email: J.Parnell@abdn.ac.uk

Orogeny involves the building of mountains by plate tectonic processes in which the lithosphere is deformed under compression. Several lines of evidence mark the Palaeoproterozoic as the time when mountain building commenced in the forms which have continued to the present day. This is evident in a rapid increase in the frequency of collisional orogens, an increase in the preservation of continental crust as recorded by the earliest large lateral plate motions, the earliest global subduction network at 2 Ga, the predominance of steep subduction zones, and the first appearance of ophiolites about 2 Ga^{1–6}. The Palaeoproterozoic also saw a marked increase in the biomass in the oceans, and consequent burial of organic carbon in the crust, which are recorded in the geochemical anomalies of the Lomagundi-Jatuli and Shunga events^{7–9}. The earliest Palaeoproterozoic carbon burial occurred at the passive margins of fragmenting supercratons as plate tectonics emerged¹⁰. The increase in abundance may have been a unique response to the c. 2.3 Ga Great Oxidation Event (GOE), and/or a series of regional responses to widespread igneous activity that provided increased nutrients^{7,11}. The result was prolific oxygen-tolerant cyanobacteria that left globally widespread carbon-rich sediment. An analysis of the time interval between the burial of organic carbon and orogeny indicates that the developments of high biomass and plate tectonics are linked. The additional carbon allowed easier deformation of the crust, in a manner that built mountain belts, and thereby plate margins characteristic of modern plate tectonics.

Results and discussion

Lubricating the growth of orogens: organic matter and mountain building. The formation of plate margins, where orogens develop, is enhanced by sediment, which confers low strength. Wet sediment and metasediment increase the lubrication of subduction^{12,13}. Sediment containing carbonaceous matter is particularly effective

in allowing deformation to occur, due to the ductile nature of organic-rich shales, overpressure weakening due to maturation of organic matter, and metamorphism to low-friction graphite¹⁴. Sediments rich in organic matter are relatively common in collisional orogens due to the incorporation of thrust platform sequences¹⁴. Consequently, numerous studies identify organic material as a critical control on the weakening of faulted rocks in orogens^{15–18}. Only small amounts (few%) of carbon are required to dominate the frictional strength of the rock and allow seismic slip¹⁹. Upon graphitization of the carbon, the frictional strength is further reduced to about 0.3 times the normal stress for carbonaceous pelitic rocks²⁰. Critically, low frictional strength enhances thrust-stacking in collisional orogens²¹, thus promoting crustal thickening during mountain building²².

Direct evidence for the deformation potential of highly carbonaceous rocks in orogens is found in an examination of major detachment surfaces in the younger Phanerozoic record. Twenty examples of thrust detachments that supported orogenic deformation (10 s to 100 s km extent), aged Cambrian to Paleogene, are consistently facilitated by shales containing a few percent TOC (Supplementary Table 1). The critical importance of this high level of organic carbon concentration to allow deformation is evident in a data set of Devonian shales ($n = 102$), where shearing occurred in shales with mean TOC 2.8%, while no shearing occurred in shales with mean TOC 1.4 %²³. When highly carbonaceous rocks occur on a global basis, their contribution to orogenic deformation is similarly widespread. Following the oceanic anoxic events of the Cretaceous, the resultant black shales became detachment surfaces in numerous orogens including in the Rockies, the Andes, Svalbard, central Europe, Indonesia, and Japan (Supplementary Table 1).

Given the link between organic matter and deformation evident in younger rocks, the scene was set for collisional orogenesis at ~2 Ga (Fig. 1) by the exceptional accumulation of

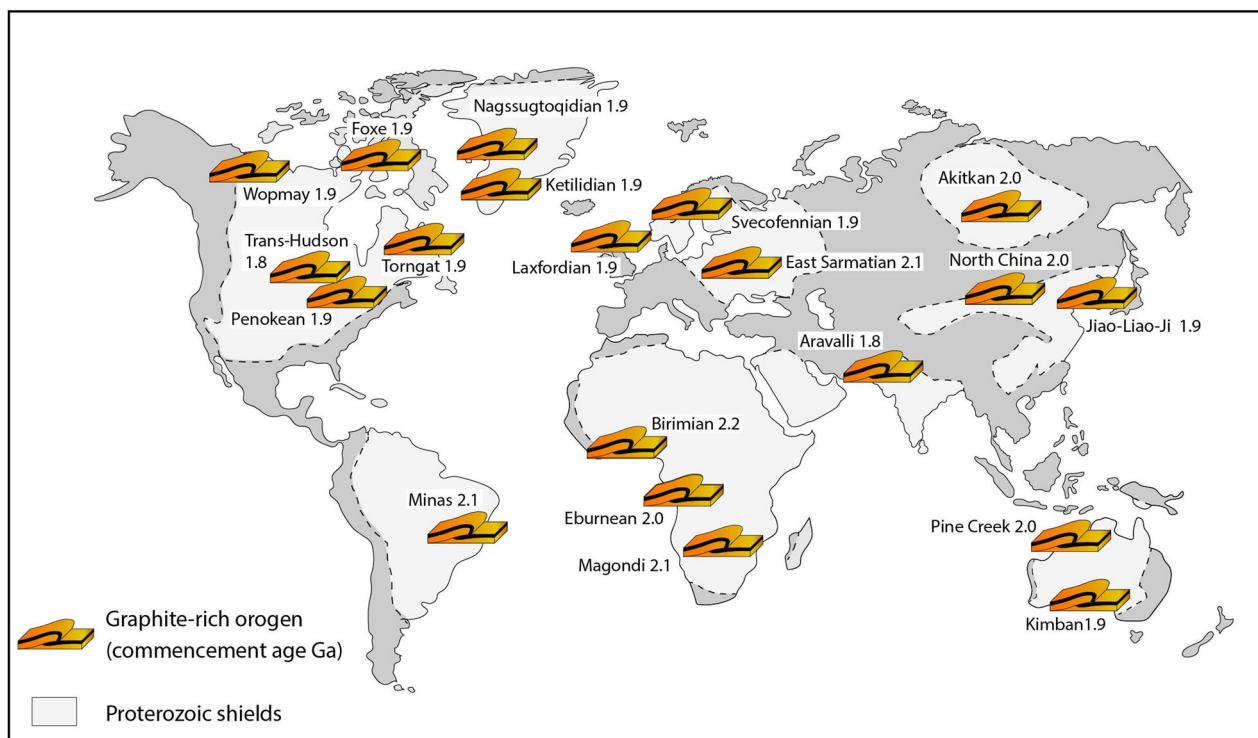


Fig. 1 Palaeoproterozoic orogens, distributed globally, exhibiting significant deformation within highly carbonaceous rocks. Orogenies all commenced 2.2 to 1.8 Ga. Details in Table 1. Orogens shown relative to distribution of Proterozoic shields⁴⁷.

organic carbon during the mid-Palaeoproterozoic (Figs. 1, 2). Abundant carbon is evident from a peak in black shale deposition²⁴, and from the record of the world's richest (highest % TOC) graphite deposits²⁵. The maximum carbon contents in carbonaceous rocks in the Palaeoproterozoic orogens are consistently above 10%, and many are above 20% (Table 1). These values are much greater than typical values for carbonaceous rocks in Phanerozoic orogens (Supplementary Table 1). Most of the richest graphite deposits are Palaeoproterozoic²⁵.

The marine cyanobacteria that are assumed to be responsible for enhanced carbon burial underwent several important developments following the GOE. Cyanobacteria became larger after the GOE, up to 50 μm diameter from <3 μm previously, and then developed sheaths²⁶, potentially increasing the mass of cellular carbon that was buried. A 10 μm diameter cell has about 25 times as much carbon as a 2.5 μm cell, based on established relationships²⁷. At this range of cell sizes, larger phytoplankton cells would also settle through the water column significantly faster, and would be more likely to flocculate⁸. This would enhance the burial of carbon by restricting the time when oxidation could occur²⁸.

In many cases, the carbonaceous sediments were accompanied by platform limestones. The stromatolite record shows a peak at ~1.9 Ga, consistent with widespread sedimentation on broad shallow platforms²⁹. The passage of anomalous quantities of carbonate into subduction zones at this time is recorded by widely distributed carbonatites in Palaeoproterozoic orogens^{30,31}. The abundant carbonate would have further reduced friction in the Palaeoproterozoic crust³². Supracrustal sediments engender thin-skinned tectonics, which is characterized by high degrees of crustal shortening^{22,33}. The wide distribution of supracrustal sediments deposited at ~2.0 Ga was therefore available to confer a high degree of shortening to the immediately subsequent orogens.

Palaeoproterozoic orogens: widespread mountain building.

A peak in orogenesis during the Palaeoproterozoic at ~2 Ga is marked by a large number of individual orogens³⁴, the overall preserved orogen length³⁴, and a high incidence of metamorphism³⁵. The first widespread formation of high mountains is inferred at this time, from a peak in the production of S-type granites from 1.95–1.65 Ga and a high incidence of metamorphic rocks³⁶.

Global deformation of the Palaeoproterozoic lithosphere is shown by the response to abundant carbon in numerous individual orogens. Twenty orogens with very highly carbonaceous rocks, of Palaeoproterozoic age distributed worldwide (Fig. 1), each record deformation focussed in pelitic/graphitic metasediments, including thrusting, imbrication, isoclinal folding, and shear zones that characterise crustal shortening (Table 1, Supplementary Note 1). The maximum period between sedimentation and deformation in the Palaeoproterozoic data set (measured from the onset of sedimentation to end of orogeny) was mostly less than 200 Myr, notwithstanding uncertainties in dating (Fig. 3; Table 1). The period ranges from 60 to 120 Myr for five orogens in North America, where more age data is available, suggesting that this is a good guide to typical times for consumption of oceanic lithosphere in the Palaeoproterozoic. Most subducting lithosphere today is Late Cretaceous or younger, with a mean age of about 65 Ma³⁷, and the time interval between Phanerozoic shale sedimentation and orogeny is usually less than 200 Myr and often less than 100 Myr (Supplementary Table 1). The consumption of seafloor sediment in the Palaeoproterozoic was, thus, at a similar rate to today, which has several implications. The similarity is consistent with the establishment of global subduction, and cycling of carbon via subduction zones,

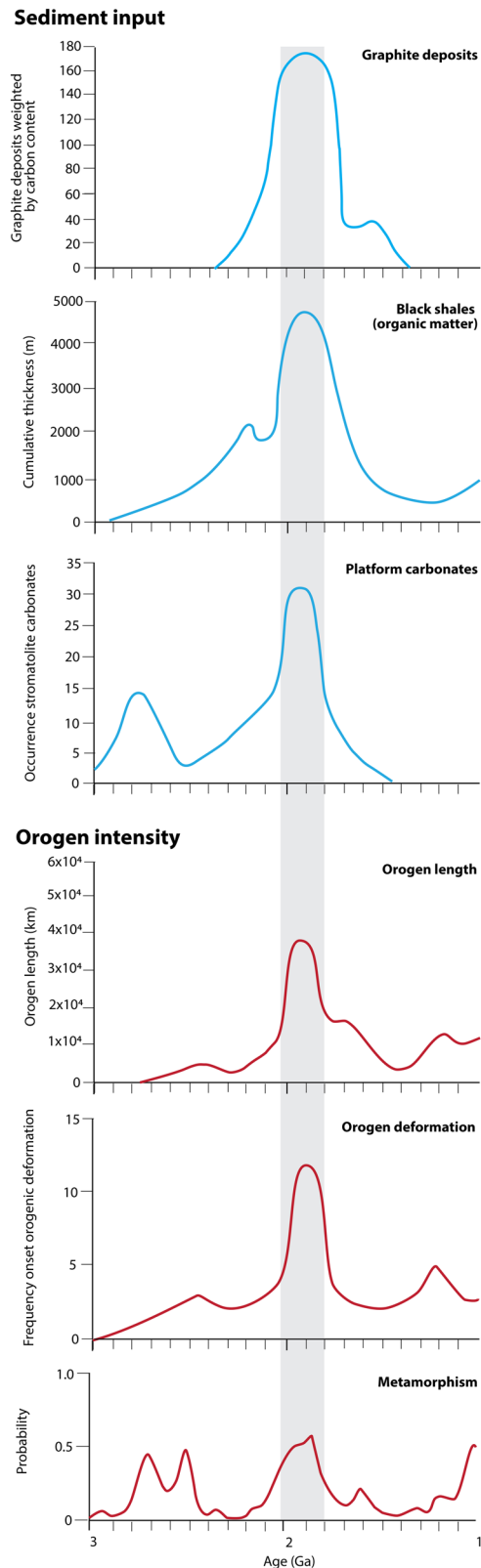


Fig. 2 Occurrence of carbonaceous sediment and orogeny through time.

Sediments (curves coloured blue) were recorded by graphite deposits weighted by mean carbon content²⁵, the abundance of black shales²⁴, and stromatolite occurrences as a measure of carbonate platform abundance²⁹. Orogeny (curves coloured red) was recorded by the incidence of metamorphism³⁵, abundance of orogens dated by the onset of deformation³⁴, and preserved length of orogens³⁴. Peak occurrence in sediment input coincides with a peak in orogenic activity, emphasized by the toned bar at 2.0 to 1.8 Ga.

Table 1 Carbon contents of carbonaceous units which accommodated deformation in orogens.

Orogen (age t_o)	Carbonaceous Unit (age t_c)	Maximum Δt ($t_c - t_o$)	Carbon content
Pine Creek Orogen, Australia (2.02-1.85 Ga)	Whites Fm. (2.02 Ga); Koolpin Fm. (1.88 Ga)	170 Myr	Up to 10.4; 11.7 % TOC
Kimban Orogen, Australia (1.85-1.70 Ga)	Hutchison Group (1.87 Ga)	170 Myr	Up to 30 + % TOC, Graphite ore
Aravalli Orogen, India (1.8-1.74 Ga)	Aravalli Supergroup (1.9-1.7 Ga)	160 Myr	Up to 15 % TOC, Graphite ore
Trans-North China Orogen, China (1.95-1.85 Ga)	Khondalite belt (2.0-1.95 Ga)	150 Myr	Up to 30 % TOC, Graphite ore
Jiao-Liao-Ji Orogen, China (1.94-1.86 Ga)	Liaohu/Jingshan Groups (2.05-1.94 Ga)	190 Myr	Graphite ore
Akitkan Orogen, Russia (2.0-1.91 Ga)	Khapchan Group, Udokan Series (2.1-1.9 Ga)	190 Myr	Up to 23 % TOC, Graphite ore
Wopmay Orogen, Canada (1.9-1.8 Ga)	Coronation Supergroup (1.88 Ga)	80 Myr	Up to 9.1 % TOC
Foxe Orogen, Canada (1.88-1.84 Ga)	Piling Group, Bravo Lake Formation (1.92-1.89 Ga)	80 Myr	Up to 5.6 % TOC
Trans-Hudson Orogen, USA-Canada (1.83-1.79 Ga)	Kisseynew Gneiss (1.85-1.84 Ga)	60 Myr	Graphite ore
Penokean Orogen, USA (1.89-1.82 Ga)	Animikie and Baraga Groups (1.88-1.83 Ga)	60 Myr	Up to 44 % TOC, Graphite ore
Tornat Orogen, Canada (1.91-1.82 Ga)	Tasiuyak Gneiss (1.94-1.88 Ga)	120 Myr	Up to 30 % TOC, Graphite ore
Nagssugtoqidian Orogen, Greenland (1.88-1.83 Ga)	Siportoq Supracrustals (2.00-1.92 Ga)	170 Myr	Up to 24 % TOC, Graphite ore
Ketilidian Orogen, Greenland (1.85-1.80 Ga)	Sortis and Vallen Groups (2.0-1.9 Ga)	200 Myr	Up to 29 % TOC, Graphite ore
Laxfordian Orogen, UK (1.9-1.87 Ga)	Lewisian supracrustals (2.0-1.9 Ga)	130 Myr	Up to 10.7 % TOC
Svecofennian Orogen, Finland-Sweden-Norway (1.88-1.79 Ga)	Multiple graphitic schists (1.91-1.88 Ga)	120 Myr	Up to 25 % TOC, Graphite ore
East Sarmatian Orogen, Belarus (2.10-2.07 Ga)	Vorontsovskaya series (2.24-2.10 Ga)	170 Myr	Up to 18 % TOC, Graphite ore
Birimian Orogen, West Africa (2.18-2.06 Ga)	Lower Birimian (2.15-2.10 Ga)	90 Myr	Up to 25 % TOC, Graphite ore
Eburnean Orogen, Gabon-Congo (2.04-2.0 Ga)	Ogooue complex, Francevillien (2.12-2.04 Ga)	120 Myr	Up to 17 % TOC
Magondi Orogen, Zimbabwe (2.06-1.96 Ga)	PiriWiri Group (2.2-2.06 Ga)	240 Myr	Graphite ore
Minas Orogen, Brazil (2.1-2.01 Ga)	Itapecerica khondalites (2.08-2.07 Ga)	70 Myr	Up to 35 % TOC, Graphite ore

TOC = Total Organic Carbon.
Data sources in Supplementary Note 1.



Fig. 3 Chronology of carbonaceous sediments and deformation in 20 Palaeoproterozoic orogens. Details in Table 1. The maximum interval between carbonaceous rocks (blue colour) and orogenic deformation (purple colour) is consistently <200 Myr, comparable to Phanerozoic orogens.

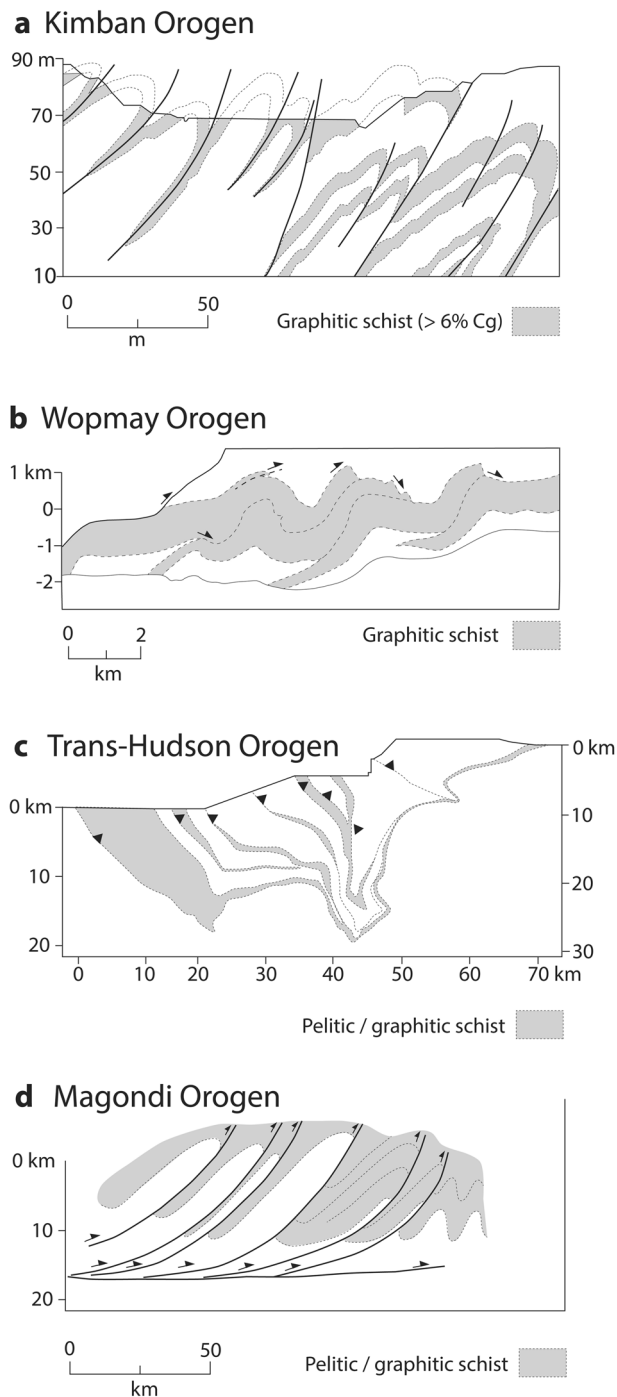


Fig. 4 Cross-sections through Palaeoproterozoic orogenic belts, deformed within pelitic/graphitic sediments. Sections in (a) Kimban, (b) Wopmay, (c) Trans-Hudson, and (d) Magondi orogens show imbricate thrust slices detached in carbonaceous sediments, commonly stacked near-vertically^{48–51}.

at ~2 Ga³. As the carbon contents of the sediment were anomalously high in the Palaeoproterozoic, the flux of carbon into subduction zones was greater, and hence deformation could take place more readily than had been possible hitherto. As inferred above, an anomalous episode of global carbon concentration on the ocean floor can support deformation by decollement in multiple orogens within 100 Myr. The availability of abundant carbon on the Palaeoproterozoic seafloor therefore

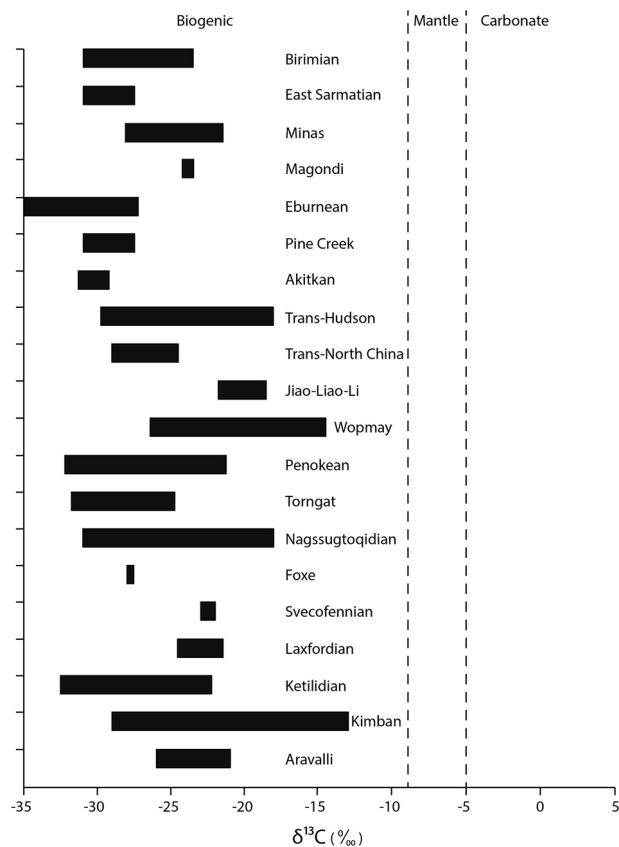


Fig. 5 Isotopic composition of carbon ($\delta^{13}\text{C}$ ‰) in carbonaceous rocks in twenty orogens. Orogens are shown in Fig. 1 and listed in Table 1. All data fall in range characteristic for biological carbon; none fall in range characteristic for magmatic carbon. Data sources in Supplementary Note 1.

allowed widespread orogenesis, as occurred subsequently in the Phanerozoic. The increasing database of ages implies a consistent speed of subduction, which supports the inference² that Palaeoproterozoic plate convergence occurred at a similar rate to the present day.

The 20 examples chosen are all collisional orogens, involving continent-continent collision, or they have a mixed accretionary and collisional history³⁴. The role played by carbonaceous rocks in contractional deformation is evident in cross-sections through Palaeoproterozoic orogenic belts, which show imbricate thrust slices detached in pelitic/graphitic sediments, often stacked near-vertically (Fig. 4).

The role of graphitic sediments in mountain building. In at least fifteen of the twenty orogens in Fig. 1, the deformed rocks contain graphite ore bodies. In ore-grade graphite, the organic carbon content is very high, enriched above the levels in unaltered carbonaceous sediments. In some cases, enrichment is a consequence of the mobilization of organic carbon during deformation and metamorphism³⁸. In some other Precambrian graphite deposits, carbon is added from mantle carbon dioxide or due to the metamorphic decarbonation of marbles³⁹. These alternatives can be distinguished by the carbon isotopic composition of the graphite, which would be relatively light or heavy, respectively³⁹. All of the twenty orogens have known isotopic compositions for their graphitic sediments, which are consistently light (Supplementary Note 1, Fig. 5), indicating a biological origin for the carbon in the orogens rather than from an abiotic source.

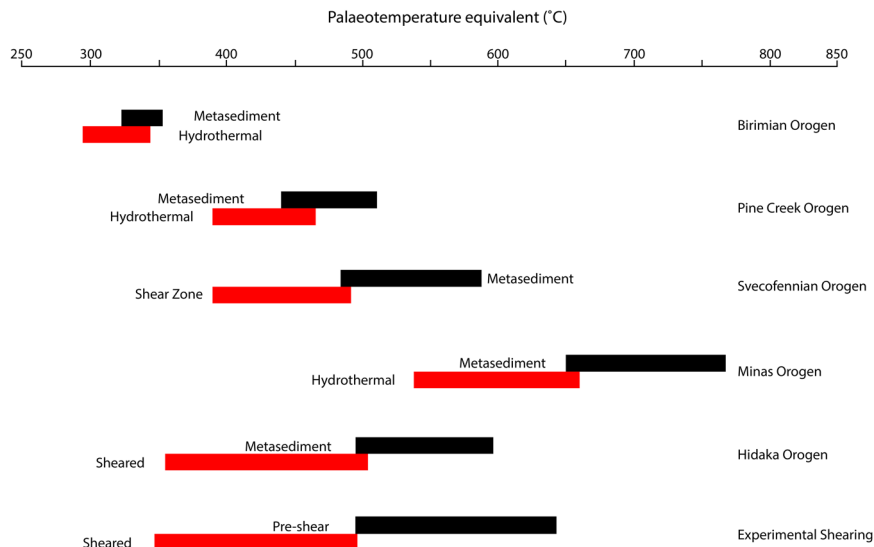


Fig. 6 Comparison of degree of order in graphitic components in metamorphic country rock and fault rock. Order is expressed as palaeotemperature equivalent, which increases with an order. Data are shown for four Palaeoproterozoic orogens^{38,41-43}, and sheared rocks in young Hidaka Orogen⁴⁰ and laboratory experiment⁵² for comparison. Orogens show decrease in order in fault rocks (red colour) relative to the original metasediment (black colour).

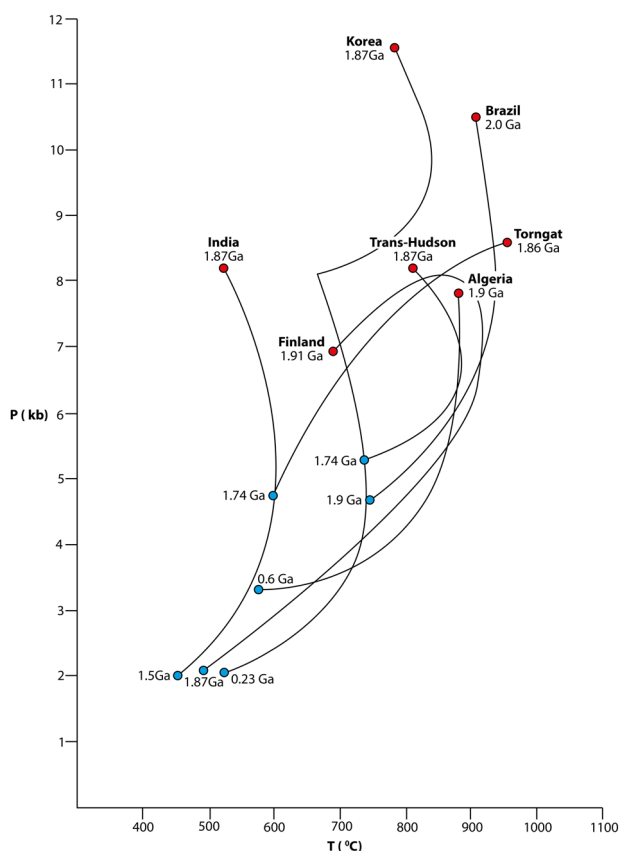


Fig. 7 Pressure-temperature (P-T) trajectories for pelitic granulites in Palaeoproterozoic orogens. Typically, trajectories pass from hot (>800 °C) temperatures (red circles) during crustal thickening to cooler temperatures (blue circles) during exhumation. Note range of timescales from thickening to exhumation from rapid to over a billion years. Trajectories from published sources⁵³⁻⁶⁰.

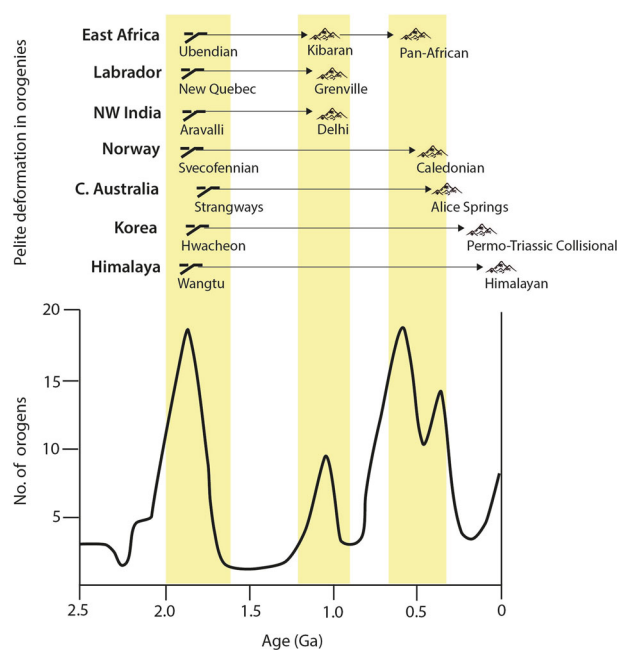


Fig. 8 Reactivation of Palaeoproterozoic pelites during younger orogenies. Pelites deformed during a subduction-related collision in the Palaeoproterozoic were deformed further during a younger continental collision, particularly during episodes of widespread orogenesis³⁴ (yellow colour). Peaks in orogen distribution are expressed as numbers of orogen lengths per 100-Myr bins⁵. Details of orogenies in Table 2.

Evidence that the graphitic sediments localized and enhanced deformation takes two forms. Firstly, the concentration of graphite on shear surfaces is a direct consequence of carbon mobility during fault slip¹⁵⁻¹⁸. In some cases (Fig. 4), there is evidence for structural thickening of the graphite due to local redistribution (e.g. in Kimban and Ketilidian orogens), and

Table 2 Examples of reworking of Palaeoproterozoic metapelites during deformation in younger orogenies (Fig. 6).

Location	Palaeoproterozoic Orogeny	Younger Orogeny
East Africa	Ubendian (metapelites 1830–1820 Ma ⁶¹)	Kibaran (1180–1090 Ma ⁶¹) Pan-African (570–550 Ma ⁶²)
Labrador	New Quebec (metapelites 1.84–1.77 Ga)	Grenville (1010 Ma ⁴⁵)
Northwest India	Aravalli (metapelites metamorphism 1.85 Ga ⁶³)	Delhi (~1000 Ma ⁶⁴)
North Norway	Svecofennian/Svecokarelian (peak metamorphism 1850 Ma ⁶⁵)	Caledonian (430 Ma ⁴⁶)
Central Australia	Strangways (sediments 1.82–1.78 Ga ⁶⁶ ; Subduction ~1.77 Ga)	Alice Springs (0.4–0.3 Ga ⁶⁷)
Korea	Hwacheon Granulite Complex (metapelites 1.87 Ga ⁵³)	Permo-Triassic Collisional (240–225 Ma ⁵³)
Himalaya	Wangtu (arc magmatism ~1.85 Ga ⁶⁸)	Himalayan (~50 Ma onwards ⁶⁸)

graphite is a noted component in subduction zones (e.g. in Trans-North China and Penokean orogens). Secondly, data from relatively young plate margins, including the Pacific rim⁴⁰, show that fault slip in graphitic rocks can cause a decrease in order in the graphite structure. This so-called strain-induced amorphization of graphite^{19,40} is an exception to the assumed irreversibility of the graphitisation process. The anomalous disorder indicates a potential signature for graphite that facilitated deformation in the deep geological record. Graphite that had been involved in deformation could be less ordered (lower maturation and inferred palaeotemperature) than the background graphitic metasediment.

Spectroscopic data from graphite in several Palaeoproterozoic orogens^{38,41–43}, including the Pine Creek Orogen (Australia), Birimian Orogen (Ghana), Minas Orogen (Brazil), and Svecofennian Orogen (Finland), distinguish between a component in the country rock representing metamorphosed organic matter, and a component in fault rocks which was mobilized from the country rock (Fig. 6). Exceptionally, the mobilized graphite in all four orogens is less ordered than the country rock, as deduced from standard measurements using Raman spectroscopy and/or X-ray diffraction, expressed as palaeotemperature-equivalents for comparison. The consistent pattern of disorder in mobilized carbon in fault rocks in the Palaeoproterozoic orogens strongly indicates that the carbon was directly involved in the Palaeoproterozoic deformation.

The long-term legacy of the Palaeoproterozoic. As the consequence of carbon burial in the Palaeoproterozoic seas was the incorporation of refractory graphite during orogenesis, much carbon became locked into the geological cycle. This left a legacy for mountain building through subsequent geological history. The properties that enhanced deformation and crustal shortening during the Palaeoproterozoic are just as likely to do so where 2 Ga sediments are present in much younger orogens. Accordingly, degrees of crustal shortening in Phanerozoic orogens are high where they are rooted in Palaeoproterozoic crust²². In the Himalayas, Palaeogene thrusting was focussed in the graphitic sediments of the ~2 Ga Lesser Himalaya Sequences, which had already focussed crustal shortening during the Palaeoproterozoic⁴⁴. The intervening 2 Gyr record includes, for example, detachment on Palaeoproterozoic shale units during the 1.0 Ga Grenvillian Orogeny in Labrador⁴⁵ and the 0.43 Ga Caledonian Orogeny in Norway⁴⁶. Pressure-temperature (P-T) trajectories for Palaeoproterozoic granulitic metapelites (Fig. 7) reflect reactivation involving compressional uplift of the granulites, either during normal exhumation or during a younger orogenic event. Palaeoproterozoic pelites were reactivated during the main periods of orogenesis over the last 2 Gyr (Fig. 8, Table 2). The exceptional Palaeoproterozoic biomass was thus reflected not only in mountain building during the Palaeoproterozoic but also in mountain building ever since.

Methods

The relationship between carbon burial and plate margin deformation was evidenced by the review of data available in the published literature.

The link was demonstrated in young (Phanerozoic) rocks using 20 case studies where detachment on organic-rich beds is documented. The case studies were characterised using the age of sedimentation, carbon contents of sediment, and age of deformation. The characterization was repeated for 20 Palaeoproterozoic orogens, with the additional documentation of organic carbon isotope composition to prove biogenicity. The periods between sedimentation and deformation were then compared between the Phanerozoic and Palaeoproterozoic data sets.

Strain composition of graphite was inferred using published spectroscopy data for carbonaceous matter in 4 Palaeoproterozoic orogens where components in the country rocks and remobilized in fault rocks were both available.

Data availability

The data tables used to produce the results of this article can be accessed at the National Geoscience Data Centre (<https://doi.org/10.5285/d10a1c96-55ff-4a35-be6b-92a4eb766b38>), entitled 'Data tables for global Palaeoproterozoic black shales', linked to NERC grant NE/M010953/1.

Received: 25 June 2021; Accepted: 22 October 2021;

Published online: 26 November 2021

References

- Abbott, D., Drury, R. & Smith, W. H. F. Flat to steep transition in subduction style. *Geology* **22**, 937–940 (1994).
- Mitchell, R. N. et al. Plate tectonics before 2.0 Ga: evidence from paleomagnetism of cratons within supercontinent Nuna. *Amer. J. Sci.* **314**, 878–894 (2014).
- Wan, B. et al. Seismological evidence for the earliest global subduction network at 2 Ga ago. *Sci. Adv.* **6**, eabc 5491 (2020).
- Weller, O. M. & St-Onge, M. R. Record of modern-style plate tectonics in the Palaeoproterozoic Trans-Hudson orogen. *Nat. Geosci.* **10**, 305–311 (2017).
- Condie, K. C. A planet in transition: the onset of plate tectonics on Earth between 3 and 2 Ga? *Geosci. Front.* **9**, 51–60 (2018).
- Brown, M. & Johnson, T. Metamorphism and the evolution of subduction on Earth. *Amer. Min.* **104**, 1065–1082 (2019).
- Martin, A. P. et al. Multiple Palaeoproterozoic carbon burial episodes and excursions. *Earth Planet. Sci. Letts.* **424**, 226–236 (2015).
- Kamennaya, N. A. et al. High pCO₂-induced exopolysaccharide-rich ballasted aggregates of planktonic cyanobacteria could explain Paleoproterozoic carbon burial. *Nat. Commun.* **9**, 2116 (2018).
- Canfield, D. E. Carbon cycle evolution before and after the great oxidation of the atmosphere. *Amer. J. Sci.* **321**, 297–331 (2021).
- Brown, M., Johnson, T. & Gardiner, N. J. Plate tectonics and the Archean Earth. *Ann. Rev. Earth Planet. Sci.* **48**, 291–320 (2020).
- Eguchi, J., Seales, J. & Dasgupta, R. Great oxidation andomagundi events linked by deep cycling and enhanced degassing of carbon. *Nat. Geosci.* **13**, 71–76 (2020).
- Behr, W. M. & Becker, T. W. Sediment control on subduction plate speeds. *Earth Planet. Sci. Letts.* **502**, 166–173 (2018).
- Sobolev, S. V. & Brown, M. Surface erosion events controlled the evolution of plate tectonics on Earth. *Nature* **570**, 52–57 (2019).
- Morley, C. K. et al. Review of major shale-dominated detachment and thrust characteristics in the diagenetic zone: Part II, rock mechanics and microscopic scale. *Earth-Sci. Rev.* **176**, 19–50 (2018).
- Rutter, E. H. et al. Reduction of friction on geological faults by weak-phase smearing. *J. Struct. Geol.* **51**, 52–60 (2013).

16. Oohashi, K., Hirose, T. & Shimamoto, T. Graphite as a lubricating agent in fault zones: an insight from low- to high-velocity friction experiments on a mixed graphite-quartz gouge. *J. Geophys. Res.* **118**, 2067–2084 (2013).
17. Craw, D. & Upton, P. Graphite reaction weakening of fault rocks, and uplift of the Annapurna Himal, central Nepal. *Geosphere* **10**, 720–731 (2014).
18. Lyu, M., Cao, S., Neubauer, F., Li, J. & Cheng, X. Deformation fabrics and strain localization mechanisms in graphitic carbon-bearing rocks from the Ailaoshan-Red River strike-slip fault zone. *J. Struct. Geol.* **140**, 104150 (2020).
19. Kaneki, S. & Hirono, T. Diagenetic and shear-induced transitions of frictional strength of carbon-bearing faults and their implications for earthquake rupture dynamics in subduction zones. *Sci. Reps.* **9**, <https://doi.org/10.1038/s41598-019-44307-y> (2019).
20. Yamasaki, S., Chigira, M. & Petley, D. N. The role of graphite layers in gravitational deformation of pelitic schist. *Eng. Geol.* **208**, 29–38 (2016).
21. Cooper, C. M., Lenardic, A., Levander, A. & Moresi, L. Creation and preservation of cratonic lithosphere: seismic constraints and geodynamic models. *Geophysical Monograph Series, Archean Geodynamics and Environments* **164**, 75–88 (2006).
22. Mouthereau, F., Watts, A. B. & Burrov, E. Structure of orogenic belts controlled by lithospheric age. *Nat. Geosci.* **6**, 785–789 (2013).
23. Enomoto, C. B., Coleman, J. L., Swezey, C. S., Niemeyer, P. W. & Dulong, F. T. Geochemical and mineralogical sampling of the Devonian shales in the Broadtop Synclinorium, Appalachian Basin, in Virginia, West Virginia, Maryland, and Pennsylvania. *U.S.G.S. Open-File Report* **2015-1061** (2015).
24. Condie, K. C., Des Marais, D. J. & Abbott, D. Precambrian superplumes and supercontinents: a record in black shales, carbon isotopes, and paleoclimates? *Precamb. Res.* **106**, 239–260 (2001).
25. Parnell, J., Brolly, C. & Boyce, A. J. Graphite from Palaeoproterozoic enhanced carbon burial, and its metallogenic legacy. *Geol. Mag.* **158**, 1711–1718 (2021).
26. Sánchez-Baracaldo, P. Origin of marine planktonic cyanobacteria. *Sci. Reps.* **5**, 17418 (2015).
27. Mullin, M. M., Sloan, P. R. & Eppley, R. W. Relationship between carbon content, cell volume, and area in phytoplankton. *Limnol. Ocean.* **11**, 307–311 (1966).
28. Chindia, J. A. & Figueredo, C. C. Phytoplankton settling depends on cell morphological traits, but what is the best predictor? *Hydrobiol.* **813**, 51–61 (2018).
29. Condie, K. C., Des Marais, D. J. & Abbott, D. Geologic evidence for a mantle superplume event at 1.9 Ga. *Geochim., Geophys., Geosyst.* **1**, GC000095 (2000).
30. Baragar, W. R. A., Mader, U. & LeCheminant, G. M. Paleoproterozoic carbonatitic ultrabasic volcanic rocks (meimechites?) of Cape Smith Belt, Quebec. *Can. J. Earth Sci.* **38**, 1313–1334 (2001).
31. Xu, C. et al. Cold deep subduction recorded by remnants of a Paleoproterozoic carbonated slab. *Nat. Commun.* **9**, <https://doi.org/10.1038/s41467-018-05140-5> (2018).
32. Kurzwski, R. et al. Earthquake nucleation in weak subducted carbonates. *Nature Geosci.* **9**, 717–722 (2016).
33. Pfiffner, O. A. Thick-skinned and thin-skinned tectonics: a global perspective. *Geosciences* **7**, 71 (2017).
34. Condie, K. C. & Puetz, S. J. Time series analysis of mantle cycles Part II: The geologic record in zircons, large igneous provinces and mantle lithosphere. *Geosci. Front.* **10**, 1327–1336 (2019).
35. Brown, M. & Johnson, T. Secular change in metamorphism and the onset of global plate tectonics. *Amer. Min.* **103**, 181–196 (2018).
36. Zhu, Z., Campbell, I. H., Allen, C. M. & Burnham, A. D. S-type granites: their origin and distribution through time as determined from detrital zircons. *Earth Planet. Sci.* **536**, 116140 (2020).
37. Seton, M. et al. A global data set of present-day oceanic crustal age and seafloor spreading parameters. *Geochem. Geophys. Geosyst.* **21**, e2020GC009214 (2020).
38. Kribek, B. et al. The origin and hydrothermal mobilization of carbonaceous matter associated with Paleoproterozoic orogenic-type gold deposits of West Africa. *Precambrian Research* **270**, 300–317 (2015).
39. Luque, F. J. et al. Vein graphite deposits: geological settings, origin, and economic significance. *Mineral. Dep.* **49**, 261–277 (2014).
40. Nakamura, Y., Oohashi, K., Toyoshima, T., Satish-Kumar, M. & Akai, J. Strain-induced amorphization of graphite in fault zones of the Hidaka metamorphic belt, Hokkaido, Japan. *J. Struct. Geol.* **72**, 142–161 (2015).
41. Mirasol-Robert, A. et al. Evidence and origin of different types of sedimentary organic matter from a Paleoproterozoic orogenic Au deposit. *Precamb. Res.* **299**, 319–338 (2017).
42. Miranda, D. A., de Oliveira Chaves, A., Campello, M. S. & de Moraes Ramos, S. L. L. Origin and thermometry of graphites from Itapeperica supracrustal succession of the southern Sao Francisco Craton by C isotopes, X-ray diffraction, and Raman spectroscopy. *Int. Geol. Rev.* **61**, 1864–1875 (2019).
43. Prando, F. et al. Fluid-mediated brittle-ductile deformation at seismogenic depth – Part 2: stress history and fluid pressure variations in a shear zone in a nuclear waste repository (Olkiluoto Island, Finland). *Solid Earth* **11**, 489–511 (2020).
44. Saha, D. Lesser Himalayan sequences in Eastern Himalaya and their deformation: Implications for Paleoproterozoic tectonic activity along the northern margin of India. *Geosci. Front.* **4**, 289–304 (2013).
45. Van Gool, J. A. M., Rivers, T. & Calon, T. Grenville front zone, Gagnon terrane, southwestern Labrador: configuration of a midcrustal foreland fold-thrust belt. *Tectonics* **27**, TC1004 (2008).
46. Torgersen, E., Viola, G. & Sandstad, J. S. Revised structure and stratigraphy of the northwestern Reparfjord Tectonic Window, northern Norway. *Norw. J. Geol.* **95**, 397–421 (2015).
47. Furnes, H., de Wit, M. & Dilek, Y. Precambrian greenstone belts host different ophiolite types. In: Dilek, Y. & Furnes, H. (eds.) *Evolution of Archean Crust and Early Life. Modern Approaches in Solid Earth Sciences* **7**, Springer Science, Dordrecht, https://doi.org/10.1007/978-94-007-7615-9_1 (2014).
48. Tirrul, R. Frontal thrust zone of Wopmay Orogen, Takiyuq lake map area, District of Mackenzie. *Current Research, Part A, Geological Survey of Canada, Paper* **82-1A**, 119–122 (1982).
49. Treloar, P. J. The geological evolution of the Magondi mobile belt, Zimbabwe. *Precamb. Res.* **38**, 55–73 (1988).
50. Lucas, S. B. & Byrne, T. Footwall involvement during arc-continent collision, Ungava orogeny, northern Canada. *J. Geol. Soc. Lond.* **149**, 237–248 (1992).
51. Keeling, J. Graphite: properties, uses and South Australian resources. *MESA J.* **84**, 28–41 (2017).
52. Kirilova, M. et al. Structural disorder of graphite and implications for graphite thermometry. *Solid Earth* **9**, 223–231 (2018).
53. Lee, S. R. & Cho, M. Metamorphic and tectonic evolution of the Hwachon Granulite Complex, Central Korea: Composite P-T path resulting from two distinct crustal-thickening events. *J. Petrol.* **44**, 197–225 (2003).
54. Van Kranendonk, M. J. Tectonic evolution of the Paleoproterozoic Torngat Orogen: evidence from pressure-temperature-time-deformation paths in the North River map area, Labrador. *Tectonics* **15**, 843–869 (1996).
55. Ouzegane, K., Bendaoud, A., Kienast, J.-R. & Touret, J. L. R. Pressure-temperature-fluid evolution in Eburnean metabasites and metapelites from Tamanrasset (Hoggar, Algeria). *J. Geol.* **109**, 247–263 (2001).
56. Bendaoud, A. et al. Geochronology and metamorphic P-T-X evolution of the Eburnean granulite-facies metapelites of Tidjenouine (Central Hoggar, Algeria): witness of the LATEA metacratonic evolution. *Geol. Soc. Lond. Spec. Pubs.* **297**, 111–146 (2008).
57. Cagnard, F., Barbey, P. & Gapais, D. Transition between “Archean-type” and “modern-type” tectonics: Insights from the Finnish Lapland Granulite Belt. *Precamb. Res.* **187**, 127–142 (2011).
58. Deshmukh, T., Prabhakar, N., Bhattacharya, A. & Madhavan, K. Late Paleoproterozoic clockwise P-T history in the Mahakoshal Belt, Central Indian Tectonic Zone: Implications for Columbia supercontinent assembly. *Precamb. Res.* **298**, 56–78 (2017).
59. Skipton, D. R., St-Onge, M. R., Schneider, D. A. & McFarlane, C. R. M. Tectono-thermal evolution of the middle crust in the Trans-Hudson Orogen, Baffin Island, Canada: Evidence from petrology and monazite geochronology of sillimanite-bearing migmatites. *J. Petrol.* **57**, 1437–1462 (2017).
60. Coelho, R. M. & de Oliveira Chaves, A. Pressure-temperature-time path of Paleoproterozoic khondalites from Claudio shear zone (southern São Francisco craton, Brazil): Links with khondalite belt of the North China craton. *J. South Amer. Earth Sci.* **94**, 102250 (2019).
61. Boniface, N., Schenk, V. & Appel, P. Paleoproterozoic eclogites of MORB-type chemistry and three Proterozoic orogenic cycles in the Ubendian Belt (Tanzania): Evidence from monazite and zircon geochronology, and geochemistry. *Precamb. Res.* **192-195**, 16–33 (2012).
62. Boniface, N. & Appel, P. Neoproterozoic reworking of the Ubendian Belt crust: implication for an orogenic cycle between the Tanzania Craton and Bangweulu Block during the assembly of Gondwana. *Precamb. Res.* **305**, 358–385 (2018).
63. Kaur, P., Zeh, A. & Chaudhri, N. Paleoproterozoic continental arc magmatism, and Neoproterozoic metamorphism in the Aravalli-Delhi orogenic belt, NW India: New constraints from in situ zircon U-Pb-Hf isotope systematics, monazite dating and whole-rock geochemistry. *J. Asian Earth Sci.* **136**, 68–88 (2017).
64. Ozha, M. K., Mishra, B., Hazarika, P., Jeyagopal, A. V. & Yadav, G. S. EPMA monazite geochronology of the basement and supracrustal rocks within the Pur-Banera basin, Rajasthan: Evidence of Columbia breakup in Northwestern India. *J. Asian Earth Sci.* **117**, 284–303 (2016).
65. Perelló, J., Clifford, J. A., Creaser, R. A. & Valencia, V. A. An example of synorogenic sediment-hosted copper mineralization: Geologic and geochronologic evidence from the Paleoproterozoic Nussir Deposit, Finnmark, Arctic Norway. *Econ. Geol.* **110**, 677–689 (2015).
66. Giles, D., Betts, P. G. & Lister, G. S. 1.8–1.5-Ga links between the North and South Australian Cratons and the Early-Middle Proterozoic configuration of Australia. *Tectonophysics* **380**, 27–41 (2004).
67. Scrimgeour, I. & Raith, J. G. High-grade reworking of Proterozoic granulites during Ordovician intraplate transpression, eastern Arunta inlier, central Australia. *Geol. Soc. Lond. Spec. Pubs.* **184**, 261–287 (2001).

68. Jain, A. K., Mukherjee, P. K. & Singhal, S. Terrane characterization in the Himalaya since Paleoproterozoic. *Episodes* **43**, 346–357 (2020).

Acknowledgements

The work was partially supported by NERC grant NE/M010953/1. The manuscript benefitted by advice from Michael Brown and Ross Mitchell.

Author contributions

Data were collated and interpreted by J.P. and C.B. Both authors have contributed to the paper, written by J.P.

Competing interests

The authors declare no competing interests.

Additional information

Supplementary information The online version contains supplementary material available at <https://doi.org/10.1038/s43247-021-00313-5>.

Correspondence and requests for materials should be addressed to John Parnell.

Peer review information *Communications Earth & Environment* thanks Michael Brown and Ross Mitchell for their contribution to the peer review of this work. Primary

Handling Editors: João Duarte, Joe Aslin, Heike Langenberg. Peer reviewer reports are available.

Reprints and permission information is available at <http://www.nature.com/reprints>

Publisher's note Springer Nature remains neutral with regard to jurisdictional claims in published maps and institutional affiliations.



Open Access This article is licensed under a Creative Commons Attribution 4.0 International License, which permits use, sharing, adaptation, distribution and reproduction in any medium or format, as long as you give appropriate credit to the original author(s) and the source, provide a link to the Creative Commons license, and indicate if changes were made. The images or other third party material in this article are included in the article's Creative Commons license, unless indicated otherwise in a credit line to the material. If material is not included in the article's Creative Commons license and your intended use is not permitted by statutory regulation or exceeds the permitted use, you will need to obtain permission directly from the copyright holder. To view a copy of this license, visit <http://creativecommons.org/licenses/by/4.0/>.

© The Author(s) 2021